Article

Pantropical moist forests are converging towards a middle leaf longevity

Meimei Xue[1,20], Xueqin Yang[1,2,20], Xiuzhi Chen [1] ✉, Philippe Ciais [3], Liming Zhou [4], Peter B. Reich [5,6], Jingfeng Xiao [7], Xing Li [8], Xiangming Xiao [9], Julia K. Green [10], Jing Ming Chen [11], Jane Liu[11], Jiali Shang[12], Xiangzhong Luo [13], Jie Tian[1], Hui Liu [14], Peng Zhu[15], Kai Yan [16], Xinyue Fu[1], Liusheng Han[17], Wenping Yuan [18] & Chaoyang Wu [19] ✉

Leaf longevity is a fundamental plant trait that largely explains ecosystem functional dynamics in global pantropical moist forests. However, the signs, magnitudes, and mechanisms of the spatiotemporal variations in leaf longevity with ongoing climate change are still lacking. Using both ground measurements and gridded leaf age-dependent leaf area index data, we map the continental-scale variability of annual mean leaf longevity across pantropical moist forests over 2001–2023. We find a biome-dependent and converging trend in leaf longevity under climate change. In Amazon and tropical Asia with long leaf longevity (> ~1.8 years), leaf longevity decreases due to rising temperature and intensified atmospheric dryness. In contrast, an increasing trend is observed in Congo and subtropical Asia where forests have short leaf longevity (<~1.8 years). These responses cause a convergence of pantropical short and long leaf longevity into a middle longevity range, with maximization of plant functional traits, photosynthesis, and species evenness, which are expected to better resist climate variability. Our study provides emerging evidence for large-scale structural and functional adaptions across pantropical moist forests and is helpful for predicting climate-driven risks to ecosystem stability.

Pantropical moist forests perform the greatest amount of terrestrial photosynthesis, driving historic land carbon sinks and potential for climate change mitigation[1]. The longevity of leaves determines the overall duration of photosynthesis for plants[2,3] and is a key feature responsible for affecting the terrestrial carbon, water, and energy fluxes in the tropics[4–6]. Leaf longevity (LL) may also affect the rate of leaf nutrient return to soil and reallocation of soil nutrients to newly flushed leaves[7], potentially regulating plant nutrient recycling[8]. Exploring the spatiotemporal variability in leaf longevity across continents is crucial for understanding plant structural and functional responses to environmental change. It is also helpful for predicting climate-driven risks to ecosystem stability.

Our knowledge of the signs, magnitudes, and mechanisms of the spatiotemporal variations in leaf longevity at large spatial scales still remains limited[9]. This gap is particularly acute for pantropical moist forests[10] that account for up to two-thirds of the approximately 73,000 tree species found on Earth[11]. Several field-based investigations demonstrated that tropical leaf longevity could vary 20-fold among sites, ranging from several weeks to more than 6 years[9,10,12–15]. Despite decades of effort to quantify leaf longevity, field measurements of large-scale leaf longevity over the long term are still lacking. Mapping the continental-scale distribution of leaf longevity in pantropical moist forests is thus highly challenging.

It is even more challenging to interpret the temporal trend in leaf longevity across pantropical moist forests, as in principle leaf longevity can either increase or decrease over time under climate change, depending on the balances between maximizing carbon gain and minimizing construction costs[16]. The leaf economics spectrum theory suggests that a longer leaf longevity allows leaves more time to fix carbon, but meanwhile increases their construction costs[16–19], which in turn results in negative feedback on leaf longevity[17,19]. Thus, pantropical leaf longevity can either be extended in response to some favorable conditions to maximize carbon gain[9,16,20–22], or be shortened by unfavorable environmental conditions[23–25]. There's a need to reconcile these seemingly opposing theoretical outcomes for leaf longevity across pantropical moist forests in the context of climate warming.

Here, we address three key research questions in this study: (1) How does leaf longevity vary across pantropical moist forests? (2) Has ongoing climate change triggered significant changes in leaf longevity across pantropical moist forests? (3) If so, do leaf longevity changes have a significant influence on leaf functional traits and plant photosynthesis or an association with plant diversity? We define leaf longevity as the inverse of leaf turnover rate (TOR), measured as the ratio of the proportions of numbers of fallen leaves (N_{fall}) and newly developed leaves (N_{new}) to total canopy leaf numbers during a certain phenological period[26,27] (Eq. 1, see "Methods"). Specifically, we used a satellite-derived leaf area index (LAI) product (2001–2023) of young (LAI_{young}) and old leaves (LAI_{old}) to quantify the proportions of fallen leaves (N_{fall}) and newly developed leaves (N_{new}) (Supplementary Figs. S1–S3). The temporal trend of leaf longevity was defined as the slope of the linear correlation between time-series annual leaf longevity and time during 2001–2023. The temporal changes in leaf longevity (ΔLL) were calculated as the difference between the first 3-year average and the last 3-year average. After that, we associated variations in satellite-derived leaf longevity data with leaf functional traits, plant photosynthesis, plant diversity and finally ecosystem resistance (defined as the proximity of the ecosystem to normal levels during a climate event[28]). Knowledge emerging from this study will be helpful for understanding plant structural and functional adaptive responses of pantropical moist forests to environmental change.

Results

Converging towards a middle leaf longevity range

We found that the magnitudes of annual mean leaf longevity varied across continents (Fig. 1). The Amazon region (LL = 2.18 ± 0.003 yrs; n = 7901) and tropical Asia (LL = 2.09 ± 0.006 yrs; n = 2198), with the most sufficient water and sunlight (Fig. 1A, B), retained the greatest leaf longevity. In contrast, the Congo region (LL = 1.28 ± 0.008 yrs; n = 2055) and subtropical Asia (LL = 1.13 ± 0.008 yrs; n = 1103) showed the shortest leaf longevity. In addition, the temporal trend in leaf longevity during 2001–2023 differs among biomes (Fig. 1C, E). Specifically, the signs of leaf longevity trends varied across pantropical moist forests with different background leaf longevity bins (Fig. 1D). Results indicated a critical middle leaf longevity range (LL_{crit} = ~1.8 yrs) below and above which contrasting leaf longevity changes were observed (LL < ~1.8 yrs: R^2 = 0.51, P < 0.001; LL > ~1.8 yrs: R^2 = 0.73, P < 0.001). Specifically, forests with leaf longevity shorter than LL_{crit} increased their leaf longevity (Congo: slope = 22 ± 2 days per decade; subtropical Asia: slope = 5 ± 2 days per decade) (Fig. 1C). Conversely, forests with leaf longevity longer than LL_{crit} shortened their leaf longevity. Approximately 69.4% of such forests were primarily found in the Amazon region (slope = − 44 ± 3 days per decade) and 27.9% in tropical Asia (slope = − 4 ± 12 days per decade) (Fig. 1C).

We then classified pantropical leaf longevity into three cohorts (short: LL < 1.5 yrs; moderate: 1.5 yrs < LL < 2.1 yrs; long: LL > 2.1 yrs) and tracked the leaf longevity transition flows among three leaf longevity cohorts during 2001–2023 using a Sankey diagram (Fig. 1F). The most noticeable change in Amazon forests was the "long-to-moderate" leaf longevity transition flow (35.3%), while the "short-to-moderate" leaf longevity transition was more evident in the Congo region (6.3%). However, in tropical and subtropical Asia, the leaf longevity transition proportions among the three leaf longevity cohorts showed approximately equal weighting. In aggregate, this transition likely led to a middle-longevity trap, showing a net decrease in both short leaf longevity cohort (LL < 1.5 yrs) (Congo: 7.5%; subtropical Asia: 3%) and long leaf longevity cohort (LL > 2.1 yrs) (Amazon: 22.3%; tropical Asia: 1.2%), with the majority shifting to the moderate leaf longevity cohort (1.5 yrs < LL < 2.1 yrs) (Fig. 1G).

Climatic driving mechanisms

The temporal changes in leaf longevity could be mostly explained by changes in climate variables (Fig. 2), as air temperature (ΔT_{air}, °C), precipitation (ΔPre, mm mon^{-1}), shortwave solar radiation (ΔSW, W m^{-2}), and atmospheric vapor pressure deficit (ΔVPD, kPa) all marked a shift in leaf longevity response below and above ~1.8 yrs (Supplementary Fig. S4A–D). The PLS-SEM analysis (GoF = 0.519) showed that, in Congo (73.9% of total pixels) and subtropical Asia (33.7% of total pixels), decreases in SW (− 0.54 ± 1.52 W m^{-2} per decade) (Supplementary Fig. S4F) had a positive impact on leaf longevity (left panel, Fig. 2A and Supplementary Fig. S5B), acting as the most important path in extending the leaf longevity in Congo and subtropical Asia (right panel, Fig. 2A). Conversely, in biomes across the Amazon and tropical Asia, the intensified VPD (0.57 ± 0.65 kPa per decade) (Supplementary Fig. S4F) had a negative impact on leaf longevity (P < 0.001, left panel in Fig. 2B and Supplementary Fig. S5D), serving as the most important path in shortening the leaf longevity in Amazon and tropical Asia (right panel, Fig. 2B). Notably, Congo and subtropical Asia had a relatively lower T_{air} (Congo: 24.88 ± 1.41 °C; subtropical Asia: 22.30 ± 3.59 °C) (Supplementary Fig. S4E). Increases in T_{air} (0.33 ± 0.21 °C per decade) (Supplementary Fig. S4F) showed a positive impact on leaf longevity across these two biomes (Fig. 2A and Supplementary Fig. S5B). Conversely, Amazon and tropical Asia experienced a relatively higher T_{air} (Amazon: 25.98 ± 2.56 °C; tropical Asia: 25.36 ± 3.23 °C) (Supplementary Fig. S4E). Rising T_{air} (ΔT_{air} = 0.20 ± 0.21 °C per decade) (Supplementary Fig. S4F) exhibited a negative impact on leaf longevity (Fig. 2B and Supplementary Fig. S5D). But the direct negative impact of T_{air} could be totally offset by its indirect positive effect via the T_{air}-VPD-LL influencing path (right panel, Fig. 2B).

The above-mentioned climatic driving mechanisms were also tested using partial correlation analyses, where the partial correlation coefficients are mostly comparable to the path coefficients of PLS-SEM analyses (Supplementary Fig. S6). The validity of their causality was also tested using the convergent cross-mapping (CCM) approach[29] (Supplementary Fig. S7). Overall, these contrasts below and above the LL_{crit} demonstrated that pantropical forests were acclimating their leaf longevity towards a middle longevity range of ~1.8 years in response to climate change.

The wide implications

The converging trend in leaf longevity might indicate potential variations in leaf functional trait values, which highly depend on leaf longevity[16]. We thus associated the structural plant traits and photosynthesis-related plant nutrient traits with leaf longevity to explore their relationships. We found that values of these structural plant traits and photosynthesis-related plant nutrient traits all peaked around LL_{crit} (Fig. 3A). Specifically, leaves with LL_{crit} exhibited highest values of structural plant traits such as leaf area (122.86 ± 2.01 cm²), thickness (0.84 ± 0.02 mm), fresh mass (3.53 ± 0.03 g), and dry mass (1.02 ± 0.01 g); and meanwhile, they also contained largest contents of photosynthesis-related plant nutrient traits such as nitrogen (2.15 ± 0.01 %), phosphorus (0.10 ± 0.01 %) and water contents (53.84 ± 0.05 %) (Supplementary Fig. S8).
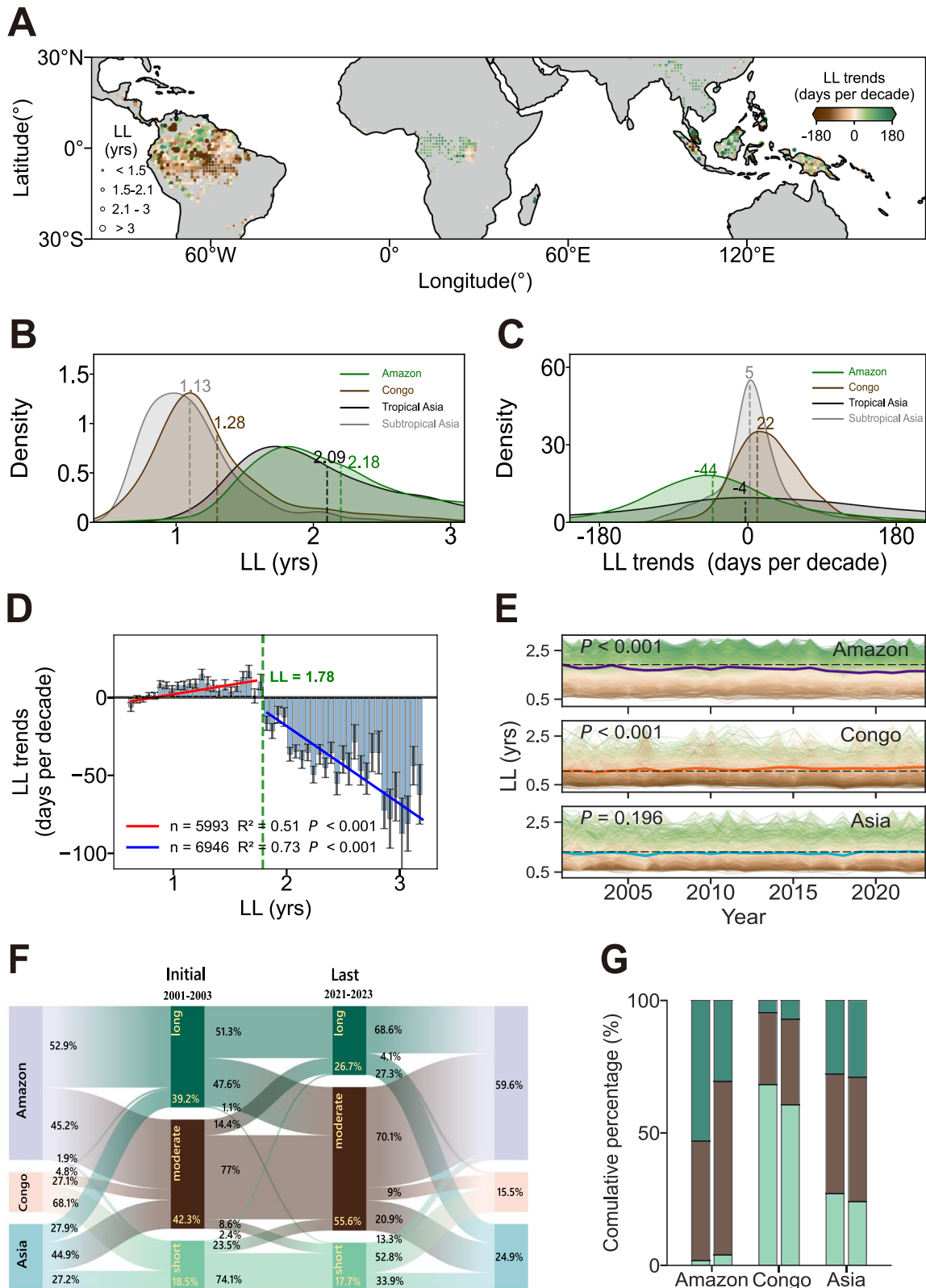
Variations in these plant functional trait values, associated with changes in leaf longevity, could further affect plant photosynthesis. Analysis of the correlation between leaf longevity and multiple satellite- and model-based GPP data (see Methods) showed that GPP reached its peak chiefly in forests with LL_{crit} (Fig. 3A and Supplementary Fig. S9). Global field observations showed that for leaves with leaf longevity below LL_{crit}, $V_{cmax,25}$ decreased with rising T_{air} (blue circle);

and on the contrary, for leaves with leaf longevity exceeding LL_{crit}, their $V_{cmax,25}$ increased with T_{air} (yellow circle) (Fig. 3B). The contrasting changes in leaf longevity were also partly associated with changes in plant community composition. We showed an inverted U-shaped relationship between leaf longevity and species evenness, with its absolute value being highest around LL_{crit} (Fig. 3C and Supplementary Fig. S10). Conversely, there was a U-shaped relationship

Fig. 1 | Satellite-observed contrasting changes in leaf longevity (LL) across pantropical moist forests. A Map of the slope of linear correlation between time-series annual leaf longevity and time during 2001–2023. The dot size indicates the annual mean leaf longevity. The color legend indicates the slope of linear correlation between time-series annual leaf longevity and time during 2001–2023. **B** The frequency distribution of annual mean leaf longevity across Amazon (green), Congo (brown), tropical Asia (black), and subtropical Asia (gray). **C** The frequency distribution of temporal changes in leaf longevity across Amazon (green), Congo (brown), tropical Asia (black), and subtropical Asia (gray). **D** Variations in the slope of the linear correlation between time-series leaf longevity and time across different background leaf longevity bins (bin = 0.05 yrs, mean ± s.e.). The leaf longevity of 1.78 yrs is the breakpoint identified in the segmented regression. The red line represents the fitting line for the interval where the leaf longevity is less than 1.78 yrs (P = 2.5e-04), and the blue line represents the fitting line for the interval

where the leaf longevity is greater than 1.78 yrs (P = 1.4e-08). The total number of samples is 12939, the number of samples in each bin is greater than 50. **E** Temporal changes in leaf longevity across Amazon, Congo, and Asia. Temporal variations in leaf longevity, showing the regional average (thick line) and values from sampled pixels (colored lines). **F** The Sankey diagram in depicting the leaf longevity transition flows among three leaf longevity cohorts (short: LL < 1.5 yrs; moderate: 1.5 yrs < LL < 2.1 yrs; long: LL > 2.1 yrs) between the initial (average from 2001 to 2003) and the last (average from 2021 to 2023) periods across the Amazon, Congo, and Asia regions. The thickness of each flow represents the number of pixels with a certain leaf longevity. **G** Proportions of three leaf longevity cohorts across the Amazon, Congo, and Asia regions, comparing the initial and the last periods (short: LL < 1.5 yrs, light green; moderate: 1.5 yrs <LL < 2.1 yrs, dark brown; long: LL > 2.1 yrs, dark green). The P-values were calculated using a two-sided Student's t test. Source data are provided as a Source Data file.

between leaf longevity and species richness, whose absolute value was smallest around LL_{crit} (Supplementary Fig. S11).

Changes in leaf functional traits, plant photosynthesis, and plant diversity that are linked to leaf longevity may have cascading impacts on ecosystem resistance (Fig. 3D). To test this, we conducted PLS-SEM analyses (LL < LL_{crit}: GoF = 0.347; LL > LL_{crit}: GoF = 0.391) to depict the potential influencing path of leaf functional traits, plant photosynthesis, and plant diversity on ecosystem resistance (see "Methods", Fig. 3E). Results showed that increases of leaf longevity in pantropical moist forests with short leaf longevity, induced by both individual acclimation and species changes, had positive impacts on forest resistance mainly through increasing their photosynthesis (path coefficient = 0.39); and conversely, decreases of leaf longevity in forests with long leaf longevity also increased their resistance mainly via enhancing functional traits (path coefficient = 0.68) (Fig. 3E).

We also adopted a space-for-time approach to establish linear correlation analysis between leaf longevity and resistance within each grid cell (12 × 12 pixels). Results showed a positive correlation between resistance and leaf longevity, where leaf longevity was below LL_{crit} (Congo: 0.07 ± 0.19; tropical Aisa: 0.03 ± 0.30) and conversely, a negative correlation between resistance and leaf longevity where leaf longevity was beyond LL_{crit} (Amazon forests: − 0.04 ± 0.19) (Supplementary Fig. S12). The correlation coefficients of partial correlation analyses among plant diversity, plant photosynthesis and leaf functional traits, and their relationships with ecosystem resistance are mostly comparable to the path coefficients of PLS-SEM analyses (Supplementary Fig. S13). The causal relationship of leaf longevity impacts on photosynthesis, functional traits and ecosystem resistance was also tested using CCM approach[29] (Supplementary Fig. S14A–C, F–H).

Discussion

The directions of ongoing shifts in leaf longevity over pantropical moist forests have been long overlooked[15,30], despite the importance of leaf longevity in influencing plant leaf physics[12], leaf chemistry[31,32], leaf traits[33], and vegetation productivity[5,34–36]. This knowledge gap is mainly due to the lack of long-term leaf longevity measurements across the pantropical moist forests[9,14]. In this study, we leveraged a newly developed leaf age-dependent LAI product to map the continental-scale decadal changes in leaf longevity. We discovered a middle leaf longevity trap in pantropical moist forests: Amazon and tropical Asia with long leaf longevity (> ~ 1.8 yrs) and Congo and subtropical Asia with short leaf longevity (< ~ 1.8 yrs) were converging towards a middle leaf longevity of ~ 1.8 yrs. The convergence in the middle leaf longevity could maximize plant leaf physics[12], leaf chemistry[31,32], leaf traits[33], ecosystem structures (species composition)[12,37,38] and functions (e.g., vegetation productivity)[9,16,20–22] in the context of climate change. Our findings highlight the importance of accounting for leaf longevity in representing tropical phenological[5,39,40] and photosynthetic processes[41], and thus in accurately predicting ecosystem dynamics in modeling scenarios[4,42,43].

In addition, the convergence in the middle leaf longevity range has important implications for plant diversity and ecosystem stability of pantropical moist forests. Species unevenness is crucial for the pantropical moist forests, where has high species richness and thus exhibit high levels of competition[44], making ecosystems less resistant to climate disturbances[45,46]. Here we show that species with leaf longevity around ~1.8 yrs in pantropical moist forests are mostly rapid-growing ones, which exhibit a small value of R_d/h_c − ratio of root depth (R_d) to canopy height (h_c) (Supplementary Fig. S15). Climate change is likely driving the biome towards low species richness and conversely high species evenness to maintain high resistance[47–50]. Nevertheless, it is worth noting that such adaption might come at the cost of functional diversity[51–53].

In summary, our study reports widespread decadal changes in leaf longevity across pantropical moist forests. Specifically, pantropical leaf longevity is changing towards a common middle range, which has the highest photosynthesis rate. Variations in leaf longevity may be closely associated with changes in plant diversity and ecosystem stability. Overall, our findings provide observational evidence to support an age-dependent all-round leaf adaptation in pantropical moist forests under climate change. Results also highlight the importance of considering leaf longevity changes when predicting climate-driven risks to plant functional traits, species diversity and ecosystem stability and have broad practical implications for improving ecosystem models.

Methods
Forest unaffected by anthropogenic and natural disturbances
In this study, we focused exclusively on the areas in pantropical moist forests (30°N ~ 30°S) that were relatively less affected by anthropogenic and natural disturbances, covering the period from 2001 to 2023. First, we identified the grid cells (0.25° resolution) always classified as evergreen broadleaf forests using MODIS MCD12C1 v061 land cover images throughout the study period[54]. We then calculated the forest cover fraction for each grid cell based on the 30 m resolution global tree cover maps from Global Forest Watch (GFW)[55]. Grid cells with forest cover fractions consistently exceeding 90% were selected as target areas. To reduce the impact of tree cover change, we concentrated our analysis on those 0.25° forest grid cells that experienced both < 2% of tree cover loss and < 2% of tree cover gain from 2000 to 2020 in each 0.25° grid cell, following the methodology outlined by ref. 56. To minimize wildfire impacts[57], we excluded grid cells containing burned areas using the MODIS Fire_cci Burned Area Pixel Product (Version 5.1) at a spatial resolution of 0.25° and a monthly temporal resolution. We focused exclusively on intact pantropical moist forests, where pixels with forest cover exceeding 90%[58].

To exclude the impacts of unusual severe dry seasons (i.e., drought events) on leaf longevity, we implemented an integrated drought assessment framework using the Palmer Drought Severity Index (PDSI)[59], the Standardized Precipitation Evapotranspiration Index (SPEI) with 6 months[60], and the Cumulative Water Deficit
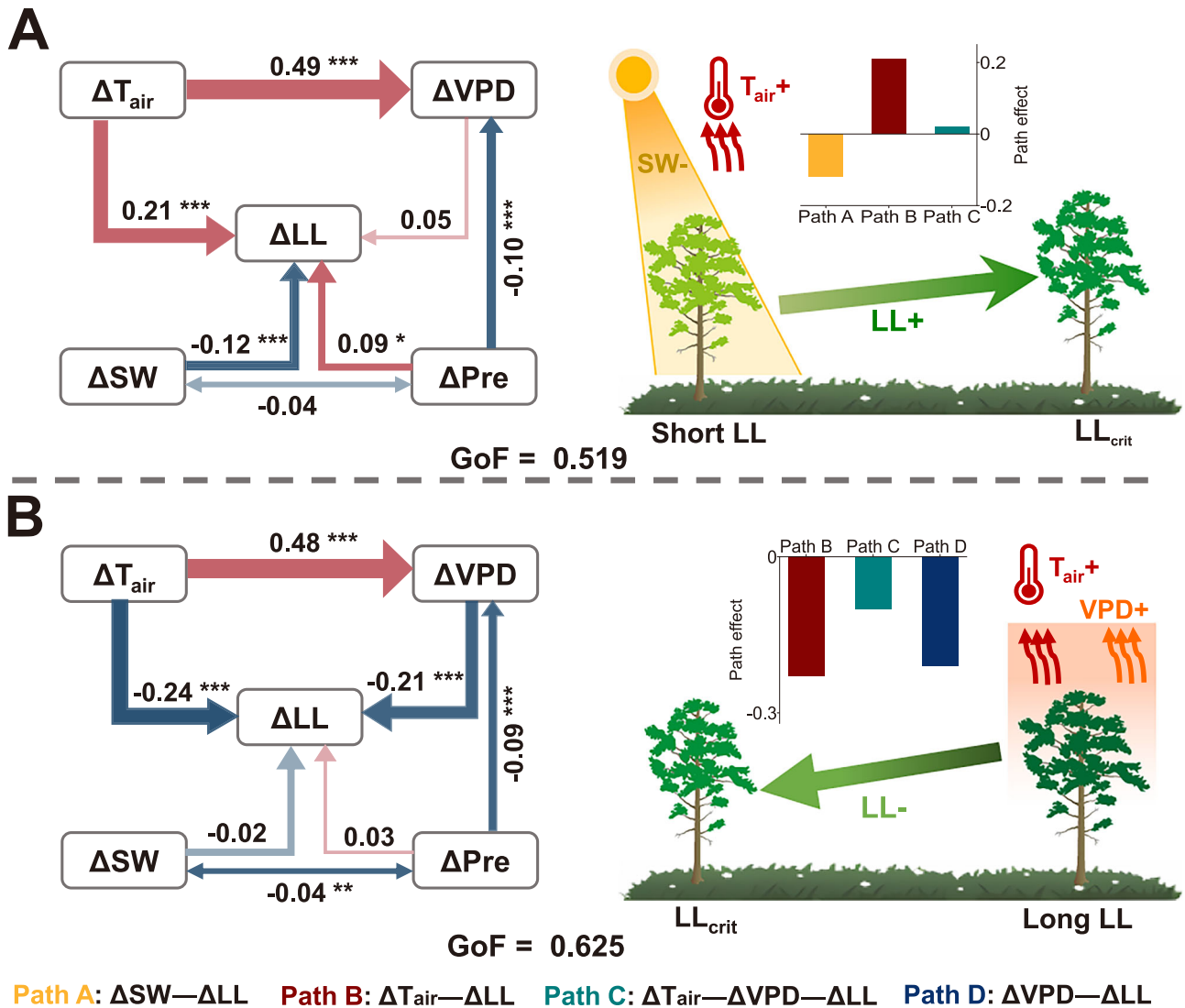
Fig. 2 | Climatic driving mechanisms for the contrasting changes in leaf longevity (LL) across pantropical moist forests. A Influences of climate variables on leaf longevity in pantropical moist forests of short leaf longevity cohorts (LL < 1.5 yrs). The left plot depicts the influencing paths of climate variability on temporal changes in leaf longevity based on the Partial Least Squares Structural Equation Modeling (PLS-SEM) analysis. The right plot shows the signs of temporal changes in those climate drivers which were responsible for the increases in leaf longevity. The inset histograms indicate the path coefficients. **B** Influences of climate variables on leaf longevity in pantropical moist forests of long leaf longevity cohorts (LL > 2.1 yrs). The left plot depicts the influencing paths of climate variability on temporal changes in leaf longevity based on the PLS-SEM analysis. The right plot shows the signs of temporal changes in those climate drivers which were responsible for the declines in leaf longevity. The inset histograms indicate the path coefficients. Asterisks indicate the significance level (two-sided Student's t test): *$P < 0.05$, **$P < 0.01$, ***$P < 0.001$. The light-colored lines represent insignificance ($P > 0.05$). Climate-driven paths include PathA (ΔSW-ΔLL, orange), PathB (ΔTair-ΔLL, dark red), PathC (ΔTair-ΔVPD-ΔLL, Teal) and PathD (ΔSW-ΔLL, dark blue). The Goodness of Fit (GoF) is an indicator for assessing the overall predictive performance of the PLS-SEM. The images of tree elements in Panels (**A**, **B**) are from the Integration and Application Network (ian.umces.edu/media-library), with image colors being modified. Source data are provided as a Source Data file.

(CWD)[61]. Specifically, a grid cell was considered to be experiencing severe drought when the annual anomalies from any of the three indices (PDSI, SPEI, or CWD) for a given year fell more than one standard deviation below their mean value of the 2001–2023 time-series[62]. We then removed forest grid cells experiencing drought events from 2001 to 2023. All data were interpolated to a spatial resolution of 0.25° to facilitate the analysis.

**Mapping the leaf longevity**

Leaf longevity is defined as the time period from leaf emergence to its shedding and fall by ref. 39, with the exclusion of exceptionally short leaf longevity resulting from accidental leaf fall caused by herbivores or other injuries. It can be quantified at the species level as the number of years required for less than half of the maximum number of leaves

to remain on a twig segment[12], or estimated at the stand level as the inverse of leaf turnover rate (TOR)[16]. The last approach allows for a comprehensive assessment of leaf longevity within the forest ecosystem[4].

In this study, we used the inverse of TOR to compute leaf longevity in pantropical moist forests. The TOR was defined as a function of the proportions of numbers of fallen leaves and newly developed leaves during a certain phenological period (Eq. 1)[26,27].

$$TOR = \frac{1}{2} \times \frac{N_{new} + N_{fall}}{N_{total} \times K_{period} \times Period} \qquad (1)$$

where TOR is the leaf turnover rate (unit: yr^{-1}). N_{new}, N_{fall}, and N_{total} are the numbers of newly developed leaves, fallen leaves, and total leaves
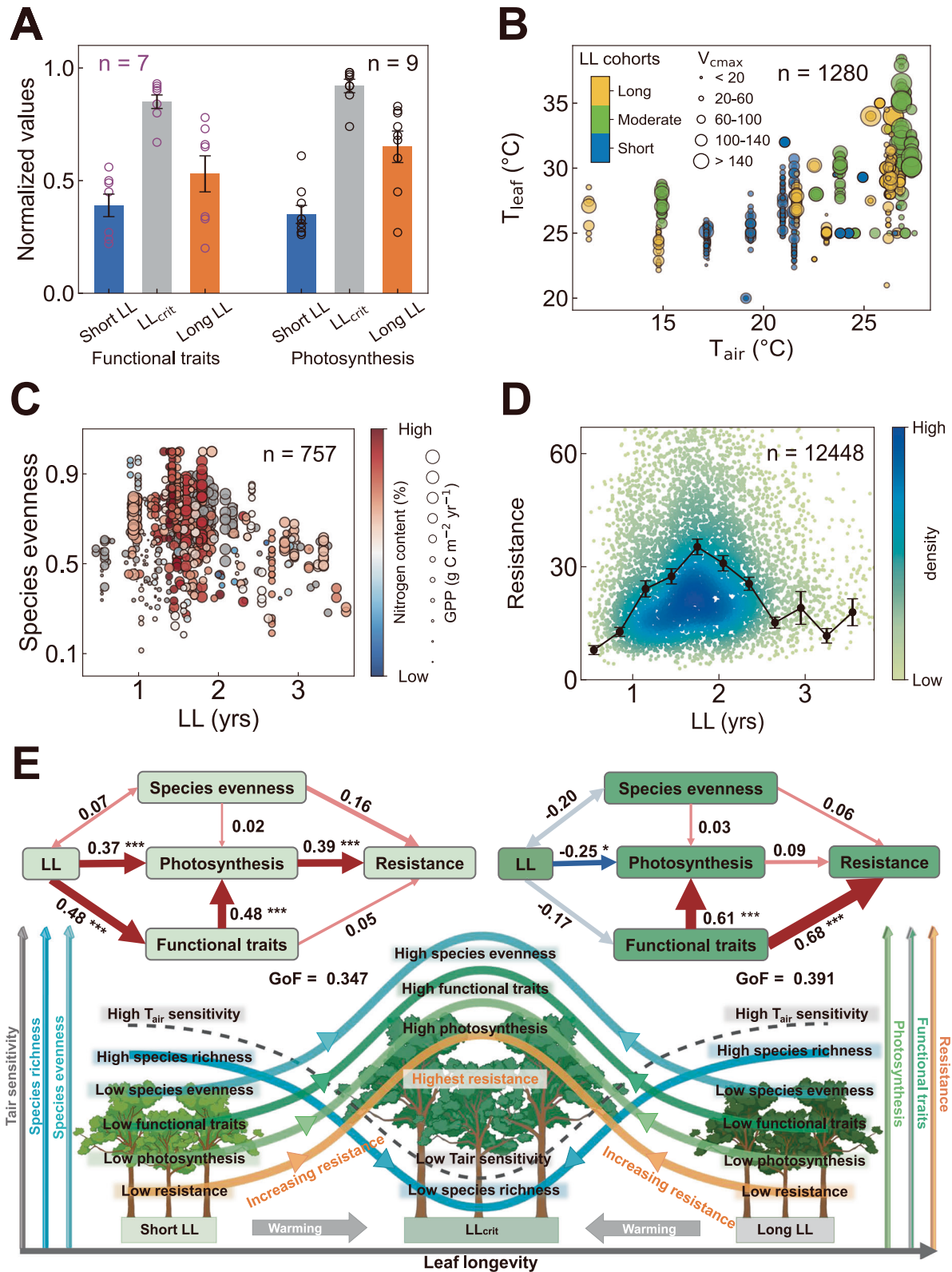
during the observation period, respectively. K_{period} is the number of phenological cycles per year for computing TOR. Period indicates the observation period (unit: yr) for N_{new}, N_{fall}, and N_{total}. The value of Period was set as 1 (yr), as calculations of N_{new}, N_{fall}, and N_{total} were conducted based on a one-year period.

In this study, we developed a leaf area index (LAI) product of old leaves (LAI_{old}) and young (LAI_{young}) for quantifying the proportions of numbers of fallen leaves (N_{fall}) and newly developed

leaves (N_{new}) (Supplementary Fig. S1). Specifically, the numbers of fallen leaves were measured as the difference between maximal LAI_{old} and minimal LAI_{old}. Conversely, the newly developed leaves were computed as the difference between the maximal LAI_{young} and the minimal LAI_{young}. Based on this, we mapped the leaf longevity data across pantropical moist forests from 2001 to 2023. The two steps for calculating leaf longevity are introduced below.

Fig. 3 | Associations of leaf longevity (LL) with plant functional traits, photosynthesis, diversity, and resistance across pantropical moist forests. A Average values of seven normalized leaf functional traits (purple) and nine normalized GPP data (black) in three leaf longevity cohorts (short: LL < 1.5 yrs, blue; moderate: 1.5 yrs <LL < 2.1 yrs, gray; long: LL > 2.1 yrs, orange). n represents the number of datasets. Refer to Supplementary Figs. S8, S9 for the scatters between functional traits and GPP data and leaf longevity. The data of seven leaf functional traits (leaf area (cm^2), thickness (mm), fresh mass (g), dry mass (g), nitrogen (N, %), phosphorus (P, %), and water contents (%)) were provided by ref. 104. The GPP data were provided by multiple satellite-based and model-estimated GPP products (see Ecological implications of leaf longevity in "Methods"): the MODIS-derived GPP[108], GOSIF-derived GPP[66], the RTSIF-derived GPP[109], FLUXCOM GPP[110], the revised EC-LUE model GPP[111], two-leaf light use efficiency (TL-LUE) model GPP[112], the vegetation photosynthesis model (VPM) GPP[113] and near-infrared reflectance of vegetation (NIRv) GPP[114]. **B** Differences in field-observed $V_{c,max25}$ and T_{leaf} under the same T_{air} conditions among the three leaf longevity cohorts (short: LL < 1.5 yrs, blue; moderate: 1.5 yrs <LL < 2.1 yrs, green; long: LL > 2.1 yrs, yellow) ($n = 1280$). The $V_{c,max25}$ and T_{leaf} data were based on in situ measurements[17]. **C** Changes of species evenness with leaf longevity across pantropical moist forests ($n = 757$). The color bar indicates the magnitude of leaf nitrogen content (gray means none value). The symbol size indicates the photosynthetic capacity of plants (GPP). The in situ plant diversity data are provided by ref. 44 (Supplementary Fig. S10). **D** Changes of resistance with leaf longevity across pantropical moist forests ($n = 12448$). Resistance was calculated by VOD using Eq. 5 (see Impacts of LL on resistance in Methods). The mean values for resistance across different background leaf longevity bins (bin = 0.3 yrs, mean ± s.e). **E** PLS-SEM analysis in depicting influences of changes in leaf longevity impact on functional traits, plant photosynthesis, plant diversity, and ecosystem resistance to disturbance in pantropical moist forests in short and long leaf longevity, respectively. Asterisks indicate significance level (two-sided Student's t test): *$P < 0.05$, **$P < 0.01$, ***$P < 0.001$. The light-colored lines represent insignificance ($P > 0.05$). The Goodness of Fit (GoF) is an indicator for assessing the overall predictive performance of the PLS-SEM. The images of tree elements in Panel (**E**) are from Integration and Application Network (ian.umces.edu/media-library), with image colors being modified. Source data are provided as a Source Data file.

Mapping LAI$_{young}$ and LAI$_{old}$ across pantropical moist forests. To map monthly LAI$_{young}$ and LAI$_{old}$ across pantropical moist forests, we classified the canopy leaves into two leaf age cohorts: photosynthetically efficient young leaves (≤ 6 months; average $V_{c,max25} = 51.4 \, \mu mol \, m^{-2} s^{-1}$) and photosynthetically less-efficient old leaves (> 6 months; average $V_{c,max25} = 41.2 \, \mu mol \, m^{-2} s^{-1}$) based on 60 field observations of leaf age and $V_{c,max25}$ in pantropical moist forests[5]. According to the Farquhar-von Caemmerer-Berry (FvCB) leaf photochemistry model[63], GPP can be expressed as a function of LAI multiplied gross primary production per leaf area (gpp). The gpp variable was the minimum of Rubisco (W_c), ribulose bisphosphate (RuBP) regeneration rate (W_j) and triose phosphate use (W_p)[9,64,65], which were calculated as functions of $V_{c,max25}$ and key climate variables [air temperature (T_{air}), shortwave solar radiation (SW), vapor pressure deficit (VPD), Carbon dioxide concentration (CO_2)] in FvCB model. In this study, we assumed that the whole-plant GPP was the sum of young leaves and old leaves. Then, GPP variable can be expressed as a function of LAI$_{young}$ and LAI$_{old}$ multiplied by their corresponding gross primary production per leaf area (gpp$_{young}$ and gpp$_{old}$), respectively (Eq. 2).

$$GPP = LAI_{young} \times gpp_{young} + LAI_{old} \times gpp_{old} \qquad (2)$$

where GPP signifies the total gross primary production. gpp$_{young}$ and gpp$_{old}$ are the average gross primary production per leaf area for leaves with leaf age equaling to 1–6 months and >6 months, respectively.

Based on this approach, we used MODIS LAI as LAI$_{total}$ to constrain the LAI$_{young}$ and LAI$_{old}$ on the right side of Eq. 2, instead of assuming a constant LAI$_{total}$ as in ref. 40. Meanwhile, data of the GPP variable were from one widely-used gridded GPP dataset (denoted as GOSIF-derived GPP)[66]. This dataset was developed from the Solar-Induced Fluorescence (SIF) measurements obtained by the Orbiting Carbon Observatory-2 (OCO-2, available since September 2014, with a spatial resolution of $1.3 \times 2.25 \, km^2$ at the ground footprint)[66]. It provided global pixel-level monthly GPP data spanning from 2000 to 2024 with a spatial resolution of 0.05°. Subsequently, in Eq. 2, LAI$_{old}$ was replaced by the term representing MODIS LAI minus LAI$_{young}$. In this situation, only one unknown variable (LAI$_{young}$) remains in Eq. 2. So, a unique value of LAI$_{young}$ was calculated for each grid cell.

Here, we used ground-based camera data of LAI$_{young}$ and LAI$_{old}$ from 10 observation sites to validate the satellite-derived LAI$_{young}$ and LAI$_{old}$ products. Results showed that they agreed well with the very fine-scale seasonality of LAI$_{young}$ and LAI$_{old}$ observed at ten sites across pantropical moist forests (Supplementary Fig. S2). Notably, the seasonality of LAI$_{young}$ and LAI$_{old}$ leaf age cohorts at K67 and K34 sites in the Amazon region was confirmed by ref. 3. The time-series camera-based observations (Barro Colorado: 2013–2016; Neon Guan:

2017–2018; ATTO: 2014–2018; Soltis: 2019–2022) also showed a strong correlation between the satellite-derived LAI age cohorts and the camera-based data (Supplementary Fig. S2). The data at Barro Colorado, Soltis, and NEON GUAN observation sites were obtained from the website[67]: https://phenocam.nau.edu/webcam/, while the data from the ATTO site were provided at ref. 68: https://doi.org/10.17871/ATTO.230.4.842. The data at Eucflux site were obtained from the website: https://phenocam.nau.edu/webcam/. The three camera-based observation sites across tropical Asia were the Banna site (provided by Qinghai Song), Ding site (provided by Juxiu Liu), and Gutian site (provided by Yanjun Du), respectively.

Calculating leaf longevity from the LAI$_{young}$ and LAI$_{old}$. The leaf area index (LAI), a proxy measuring the total one-sided green leaf area per unit of ground surface area, can represent the number of leaves in plants to some extent[69,70]. Thus, we computed the difference between maximal LAI$_{old}$ and minimal LAI$_{old}$ to define N$_{fall}$ and computed the difference between maximal LAI$_{young}$ and minimal LAI$_{young}$ to define N$_{new}$. The total numbers of leaves were represented as MODIS LAI. Based on this, we mapped the annual leaf longevity data across pantropical moist forests from 2001 to 2023. Notably, there were three types of periodic phenology across pantropical moist forests: annual (12-months) unimodal phenology, half-year (6-month) bimodal phenology and phenology between the first two[71]. When $R_1 > 90\%$, corresponding pixels show a unimodal (12-month) phenology, where R_1 represents the phenological proxy occurring once per year, and this type of phenology is defined as an annual cycle. R_2 represents the phenological proxy occurring twice per year, when R_2 is bigger than 50%, their phenology shows a half-year (6-month) cycle[72]. For the remaining pixels, the larger the R_1 value is, the greater the probability the phenology is close to the unimodal annual cycle phenology; the smaller the R_1 value is, the greater the probability the phenology is close to the half-year cycle phenology. Then, for each grid cell, the number of phenological cycles per year (K$_{period}$) was determined based on local leaf phenology patterns, ranging from 1 to 2. Specifically, for grid cells with an annual (12-months) unimodal phenology cycle, K$_{period}$ was set to 1. For grid cells with half-year (6-months) bimodal phenology cycle, K$_{period}$ was set to 2. When the bimodal phenology is close to a half-year cycle (i.e., $50\% < R_1 < 60\%$), K$_{period}$ was set to 1.8. When R_1 was between 60% and 70%, K$_{period}$ was set to 1.6; R_1 between 70% and 80%, K$_{period}$ was set to 1.4. When the bimodal phenology is close to the annual cycle (R_1 between 80% and 90%), K$_{period}$ was set to 1.2. Using this method, annual leaf longevity for each pantropical moist forests grid cell was estimated.

To test the robustness of our analysis, we used other two alternative nearby thresholds of K$_{period}$ [($50\% < R_1 < 60\%$: K$_{period}$ = 1.7; $60\% < R_1 < 70\%$: K$_{period}$ = 1.5; $70\% < R_1 < 80\%$: K$_{period}$ = 1.3; $80\% < R_1 < 90\%$:

$K_{period} = 1.1$); (50% < R_1 < 60%: $K_{period} = 1.9$; 60% < R_1 < 70%: $K_{period} = 1.7$; 70% < R_1 < 80%: $K_{period} = 1.5$; 80% < R_1 < 90%: $K_{period} = 1.3$)] to reconstruct leaf longevity. Both two newly- reconstructed leaf longevity datasets showed consistent leaf longevity trends (Supplementary Fig. S16).

Validation of satellite-based leaf longevity using global in situ data.
Our satellite-derived leaf longevity products were comprehensively validated by 18 samples of in situ leaf longevity measurements across pantropical moist forests (Supplementary Fig. S3). Overall, 77.8% of the validations fell into the 95% confidence interval ($R = 0.86$; RMSE = 0.34) (Supplementary Fig. S3B). Records of the longitude, latitude, and in situ leaf longevity measurements were listed in Supplementary Data S1 (Supplementary Data 1).

In addition, we also used 117 samples of leaf longevity data estimated from camera-based LAI age cohort data ($n = 7$) and in situ LMA data ($n = 110$) across tropical moist forests (Supplementary Fig. S3 and Supplementary Data S2, S3 in Supplementary Data 1).

Notably, the seasonality of LAI_{young} and LAI_{old} from K67, K34, Eucflux, Banna, Ding and Gutian sites was used to validate the gridded leaf longevity dataset. We first calculated the N_{new} (N_{fall}), then we calculated camera-based leaf longevity from N_{new} and N_{fall} from Eq. 1. Overall, 57.1% of the validations fell into the 95% confidence interval (Supplementary Fig. S3C). The camera-based seasonality of LAI_{young}, LAI_{old} and leaf longevity data was listed in Data S2 (Supplementary Data 1).

Previous studies have shown a linear relationship between $log_{10}(LMA)$ and $log_{10}(LL)$ (Eq. 3)[2,9,19]. Overall, 72.7% of the validation points fell into the 95% confidence interval (Supplementary Fig. S3C). The information of in situ LMA data and estimated leaf longevity data was listed in Supplementary Data S3 (Supplementary Data 1).

$$log_{10}(LL) = log_{10}(LMA) + b \qquad (3)$$

where b is a parameter to calibrate the overall simulation accuracy. It was set as a value of 0.90 according to observed LMA and leaf longevity data across pantropical moist forests[2,9,19].

Sankey diagram for leaf longevity transitioning flow
The Sankey diagram is a data visualization technique that highlights transitions, movement, or change from one state to another, with the width of the arrows proportional to the flow rate of the depicted property[73,74]. In this study, Sankey diagram was used to trace the transition process between different cohorts of leaf longevity in different regions from the initial state to the last state during the study period (Fig. 1F). First, we divided the studied pantropical moist forests into three cohorts according to different leaf longevity thresholds, namely long (LL > 2.1 yrs), moderate (1.5 yrs < LL < 2.1 yrs) and short (LL < 1.5 yrs) leaf longevity cohorts. Then, we calculated the proportions of pixels with long, moderate, and short leaf longevity for the initial (the first 3-year average) and final (the last 3-year average) time periods, and established the Sankey diagram to represent the transition flows between different cohorts of leaf longevity. The thickness of each flow represents the number of pixels with a certain leaf longevity. The value of each flow represents the proportions of three leaf longevity cohorts in initial (the first 3-year average) and final (the last 3-year average) periods. Notably, the Sankey diagram analysis was established in three main tropical regions, including the Amazon, the Congo and Asia.

The robustness of using 1.5 yrs and 2.1 yrs as thresholds to classify the long, moderate, and short leaf longevity for Sankey diagram analysis were also tested by other two alternative nearby thresholds: 1.4 yrs < LL < 2.2 yrs and 1.6 yrs < LL < 2.0 yrs. Consistent transition flows among three leaf longevity cohorts were observed (Supplementary Fig. S17).

Paths of climatic factors in leaf longevity
PLS-SEM is a robust statistical technique designed to analyze complex cause-effect relationships in path models, which include latent variables[75]. It combines principal component analysis with regression-based path analysis[76]. It allows testing of hypothesized relationships while maintaining a focus on prediction during model estimation[77,78]. One effective indicator for assessing the overall predictive performance of PLS-SEM is the Goodness of Fit (GoF)[79]. GoF refers to the evaluation of how well a model fits the observed data, typically calculated using the chi-square quantity, which compares the applied forces to the fitted forces estimated by the least squares method[80]. GoF values above 0.7 are considered very good, while those above 0.5 are considered good[81].

In our study, we employed a straightforward PLS-SEM model that included four key climate variables [annual mean air temperature (T_{air}, °C), solar shortwave radiation (SW, W m^{-2}), atmospheric vapor pressure deficit (VPD, kPa), precipitation (Pre, mm mon^{-1})], to explore their effects on leaf longevity (Fig. 2). We utilized the T_{air} data from Terra-Climate dataset[82], spanning the period from 1958 to present, with monthly temporal resolution and a ~ 4 km (1/24th degree) spatial resolution. Breathing Earth System Simulator (BESS) is a simplified process-based model that couples the atmosphere and canopy radiative transfers, canopy photosynthesis, transpiration, and energy balance. The SW data were obtained from BESS[83], spanning the period from 2000 to 2021, with daily temporal resolution and a 0.05° spatial resolution. The VPD data were sourced from the ERA5-Land reanalysis dataset[84], with monthly temporal resolution (1950-present) and a spatial resolution of 0.1°. The Pre data were obtained from the Tropical Rainfall Measuring Mission Project (TRMM/3B43) dataset version 7[85], which have monthly temporal resolution (1998–2020) and a spatial resolution of 0.25°.

Climatic drivers of leaf longevity
The Random Forest (RF) algorithm[86–89] aggregates multiple Classification and Regression Tree (CART) algorithms using bootstrap aggregation (bagging) and enhances predictive accuracy while reducing overfitting and sensitivity to irrelevant predictors[90]. These advantages make RF particularly suitable for ecological applications, where environmental drivers often exhibit complex interactions and spatial heterogeneity.

A key feature of RF models is their ability to quantify the relative influence of environmental variables through Variable Importance Measures (VIM). This metric, derived from a permutation-based approach, evaluates the contribution of each predictor by measuring the decrease in model performance when its values are randomly shuffled[85]. VIM provides an objective ranking of environmental drivers, allowing us to identify the most influential factors governing spatial and temporal variations in leaf longevity. Importantly, this method maintains robustness against measurement uncertainties, making it well-suited for ecological datasets characterized by high variability and observational noise[91,92]. The VIM values were calculated following Eq. 4, providing a quantitative basis for assessing the role of each environmental variable in shaping leaf longevity dynamics:

$$VIM(x_j) = \sum_{t=1}^{T} \frac{n_t}{N} \Delta Gini\left(S(x_j, t)\right) \qquad (4)$$

where n_t denotes the number of observations belonging to node t within the tree. n represents the total number of observations, and T denotes the total number of nodes. The climatic drivers influencing leaf longevity are represented by x_j variables. The $\Delta Gini$ is defined as the difference between the calculated Gini index[93] at node t and its parent node (Eq. 4). The mean error rate ($S(x_j, t)$) across all out-of-bag observations before permuting predictor j was used to estimate the unbiased importance of each variable[94].

To further interpret the relationships between climate variables and leaf longevity variations, we employed Partial Dependence Plots (PDPs)[95], which illustrate the marginal effect of each predictor on leaf longevity while accounting for its interactions with other variables. The PDPs allowed us to distinguish positive and negative correlations between climate drivers and leaf longevity across temporal scales. We estimated changes in leaf longevity (ΔLL) for each forested pixel in the pantropical moist forests by calculating the difference between the mean leaf longevity values for 2021–2023 and 2001–2003. These mean values were calculated from the linear regression trend over the full time series. Climate variable changes were computed using the same approach. An RF model was then built with ΔLL as the response variable and climate changes as predictors. The VIM values were derived to rank the relative importance of each climate driver, while PDPs were generated to visualize their individual effects on ΔLL (Supplementary Fig. S5), providing insights into the contributions of climate variability to temporal trends in leaf longevity. The CART and PDP analyses were implemented from the Partial Dependence Display module of the scikit-learn package in Python (https://scikit-learn.org/stable, last accessed: 10 Oct. 2023). This study focuses on several key climate variables, including atmospheric carbon dioxide concentration (CO_2), mean air temperature parameters (T_{air}), precipitation (Pre), surface downwelling shortwave radiation flux (SW) and vapor pressure deficit (VPD). These factors have been widely recognized as critical regulators of ecological processes, influencing leaf phenology[96,97], leaf traits[98,99], carbon and water cycle[100,101], and tree mortality[102,103] across pantropical moist forests.

Ecological implications of leaf longevity
Exploring the impacts of leaf longevity functional traits. Aguirre-Gutiérrez et al. (2025)[104] combined field-collected data from more than 1,800 vegetation plots and tree traits with satellite remote-sensing data (European Space Agency Sentinel-2 satellite data), terrain (slope), climate (maximum climatic water deficit and maximum temperature) and soil (clay percentage, sand percentage, pH and cation-exchange capacity) data to predict 13 tree functional traits, spanning leaf morphological (leaf area, specific leaf area, thickness, fresh and dry mass, leaf water content), chemical (mass-based calcium, carbon, magnesium, nitrogen, potassium, phosphorus concentrations) traits and wood density[104]. These plant traits were gathered from tropical forests across the Americas, Africa and Asia. All plant functional traits used were part of the Global Ecosystems Monitoring network (GEM)[105], the MONAFOR network, the ForestPlot[106], BIEN and TRY[107] databases and from local collaborators.

Here, we selected seven plant functional traits that were related to photosynthesis, provided by ref. 104 to analyze with leaf longevity (Fig. 3A and Supplementary Fig. S8). The seven plant functional traits included: leaf area (cm^2), leaf thickness (mm), fresh and dry mass (g), leaf water content (%), nitrogen (N, %), phosphorus (P, %) concentrations. To ensure comparability, all plant functional traits maps were resampled to 0.25° spatial resolution

Exploring the impacts of leaf longevity photosynthesis. We first selected nine satellite-derived or model-simulated GPP datasets to compare the differences in photosynthetic capacity of leaves with different leaf longevity (Fig. 3A and Fig. S9). They included: the MODIS-derived GPP[108], GOSIF-derived GPP[66], the RTSIF-derived GPP[109], FLUX-COM GPP[110], the revised EC-LUE model GPP[111], the two-leaf light use efficiency (TL-LUE) model GPP[112], the vegetation photosynthesis model (VPM) GPP[113] and near-infrared reflectance of vegetation (NIRv) GPP[114].

Notably, MODIS GPP (MOD17A2H v006) was generated at the native resolution of 500 m using the Moderate Resolution Imaging Spectroradiometer (MODIS) Leaf Area Index(LAI)/Fraction of Photosynthetically Active Radiation (FPAR) (MOD15A2H) 8-day composite at 500 m resolution, which spans from 2000 to 2023[108]. RTSIF-derived

GPP at a spatial resolution of 0.05° and a temporal resolution of 8 days, spanning from 2001 to 2020, was derived from TROPOMI (Tropospheric Monitoring Instrument) SIF data, according to the relationships between the SIF and GPP delineated by ref. 109, which used a constant value of 15.343 to transform the SIF to the GPP. FLUXCOM GPP data were developed using a machine learning approach to merge carbon flux measurements from FLUXNET eddy covariance towers with remote sensing and meteorological data[110]. In the remote sensing and meteorological data (RS + METEO) setup, fluxes were estimated from meteorological data and mean seasonal cycles of satellite data. For the RS + METEO products, the trained machine learning models were applied to the gridded predictor variable fields for a daily time step with a spatial resolution of 0.5°. In this paper, two kinds of machine learning models, artificial neural network (ANN) and multiple adaptive regression spline (MARS) in RS + METEO products, were selected for analysis. The revised EC-LUE GPP data, developed based on the revised light utilization efficiency model (i.e., the EC-LUE model), has a spatial resolution of 0.05° and an interval of 8 days, and its time range is from 1982 to 2018[111]. In the revised EC-LUE model, several major environmental variables such as atmospheric CO_2 concentration, radiation composition and atmospheric vapor pressure deficit (VPD) were integrated. Based on the updated TL-LUE model, a global 0.05°, 8-day GPP dataset for 1992–2020 was generated using GLOBMAP leaf area index, CRUJRA meteorology, and ESA-CCI land cover data[112]. The VPM GPP dataset has moderate spatial (500 m) and temporal (8-day) resolutions over the entire globe for 2000–2016[113]. This GPP dataset was driven by satellite data from MODIS and climate data from NCEP Reanalysis II. Near-infrared reflectance of vegetation (NIRv) is a remotely sensed measure of canopy structure, which can accurately predict the photosynthesis at FLUXNET validation sites on a monthly to annual time scale, which is calculated by the product of Normalized Difference Vegetation Index (NDVI) and near-infrared (NIR) reflectance (NDVI × NIR). NIRv GPP is generated by cross-referencing monthly and annual GPP fluxes from flux sites that meet quality control requirements and fall within the temporal coverage of MODIS records (2001-present)[114]. The methodology for estimating NIRv GPP was systematically upscaled from site-level observations to a globally applicable framework. To ensure comparability, all GPP products were resampled to 0.25° spatial resolution and aggregated to the same time scale.

Then, our satellite-derived leaf longevity data were further analyzed against ground-measured maximum carboxylation rate ($V_{c,max25}$) and temperature records. We collected 1280 $V_{c,max25}$ measurements together with the leaf temperature (T_{leaf}) data from 62 sites across whole pantropical moist forests (Fig. 3B). The observational dataset integrates top-canopy measurements from natural vegetation[17], with $V_{c,max25}$ values derived either from the net photosynthesis (A_{net})-intercellular CO_2 (C_i) response curves or via the one-point method (method presented in ref. 115). The dataset also includes latitude, longitude and leaf temperature at the time of measurement for each sample. Corresponding air temperatures (T_{air}, °C) for each sample were extracted from monthly, 1901–2015, 0.5° resolution data provided by the Climatic Research Unit (CRU TS3.24.01) according to the location of each observation site[116]. Based on this field dataset, we implemented a bivariate scatterplot analysis integrating four key variables, including T_{air}, T_{leaf}, $V_{c,max25}$, and leaf longevity (Fig. 3B). These dual visual encoding analyses permitted simultaneous assessment of thermal niches and photosynthetic performance across leaf longevity gradients.

Associating leaf longevity with plant diversity. Biodiversity is an important component of natural ecosystems, and species richness and evenness are two key indicators of biodiversity. Thus, we used species richness and species evenness to analyze the plant diversity differences of forests with different leaf longevity conditions (Fig. 3C,

Supplementary Figs. S10, S11). The species evenness data used in this paper were provided by ref. 44. And the species richness data were from the global forest diversity (GFB) map collected by ref. 117. The GFB data came from in situ remeasurements of 777,126 permanent sample sites in 44 countries and territories and 13 ecological regions, most of which were taken from two successive inventories of the same site. Notably, species richness and evenness were usually negatively correlated across forests globally.

Impacts of leaf longevity on resistance

In this study, we quantified resistance based on the Ku-band Vegetation optical depth (VOD)[118] and computed the forest resistance as the dimensionless ratio between baseline vegetation status and greenness reductions during extreme temperature events[119,120] (Eq. 5). Extreme climate events were identified by detecting the minimum VOD value in the detrended VOD anomalies time series spanning 2001–2017, with detrending via the linear regression method. The VOD value during the extreme temperature events was designated as Y_e, while $\bar{Y}_n$ was derived from the multi-year mean VOD for corresponding calendar months in non-disturbance years. In this study, we only selected those relative to extreme temperature events for analyses.

$$\text{resistance} = \frac{\bar{Y}_n}{|Y_e - \bar{Y}_n|} \qquad (5)$$

where resistance represents forest resistance to climate disturbance, $\bar{Y}_n$ denotes baseline vegetation status (value of VOD) under undisturbed conditions, Y_e represents vegetation state during an extreme climate event.

After mapping the resistance (Supplementary Fig. S12A), we analyzed the variations of resistance with leaf longevity across pantropical moist forests (Fig. 3D). Then, we employed a straightforward PLS-SEM model that included leaf functional traits, photosynthesis (i.e., GPP), and plant diversity (i.e., species evenness) to depict how leaf longevity impacts on resistance (Fig. 3E). We also adopted a space-for-time approach[56] to establish linear correlation analysis between leaf longevity and resistance within each 12 × 12 grid cell, by limiting potential influences from climate variability. Results revealed an inverted U-shaped relationship between annual mean resistance and leaf longevity, with the parabola vertex sited around LL_{crit} (Supplementary Fig. S12B, C).

Reporting summary

Further information on research design is available in the Nature Portfolio Reporting Summary linked to this article.

Data availability

All the relevant data in this study come from publicly available sources as follows: MODIS MCD12C1 Land Cover images: https://lpdaac.usgs.gov/products/mcd12c1v061/; Global Forest Watch (GFW) tree cover images: https://glad.earthengine.app/view/global-forest-change; MODIS Fire_cci Burned Area Pixel product, version 5.1: https://catalogue.ceda.ac.uk/uuid/3628cb2fdba443588155e15dee8e5352/; SPEI01 base v2.6: https://spei.csic.es/database.html; Terraclimate PDSI and Tair data: https://www.climatologylab.org/terraclimate.html; TRMM Pre data: https://disc.gsfc.nasa.gov/datasets/TRMM_3B43_7/summary?keywords=TRMM; ERA5-Land VPD data: https://cds.climate.copernicus.eu/datasets/reanalysis-era5-land-monthly-means?tab=overview; Bess SW data: https://www.environment.snu.ac.kr/bess-rad; CO2 dataset: https://www.geodoi.ac.cn/edoi.aspx?DOI=10.3974/geodb.2021.11.01.V1; MODIS-GPP: https://lpdaac.usgs.gov/products/mod17a2hv006/; GOSIF-GPP: http://data.globalecology.unh.edu/data/GOSIF-GPP_v2/; RTSIF: https://figshare.com/articles/dataset/RTSIF_dataset/19336346/2; FLUXCOM RS + METEO GPP: https://www.bgc-jena.mpg.de/geodb/projects/Home.php; EC-LUE Model GPP: https://doi.org/10.6084/m9.figshare.8942336.v3; TL-LUE Model GPP: https://nesdc.org.cn/sdo/detail?id=671486ad7e28174998399e5d; VPM GPP: https://doi.org/10.6084/m9.figshare.c.3789814; plant functional traits map: https://pantropicalanalysis.users.earthengine.app/view/pantropical-traits-aguirre-gutierrez-2025; Ku-VOD: https://zenodo.org/records/2575599; Global Biodiversity Information Facility (GBIF): https://www.gbif.org/zh/species/search. The leaf longevity data generated in this study have been deposited in the Figshare database under accession code: https://doi.org/10.6084/m9.figshare.30750074. All in situ data that validate the leaf longevity data of this study are available in the Supplementary Data file. Source data are provided in this paper.

Code availability

The code in this study is archived on Zenodo at https://doi.org/10.5281/zenodo.17336535.

References

1. Lai, J. et al. Terrestrial photosynthesis inferred from plant carbonyl sulfide uptake. *Nature* **634**, 855–861 (2024).
2. Wright, I. J. et al. The worldwide leaf economics spectrum. *Nature* **428**, 821–827 (2004).
3. Wu, J. et al. Leaf development and demography explain photosynthetic seasonality in Amazon evergreen forests. *Science* **351**, 972–976 (2016).
4. Zhang, H., Liu, D., Dong, W., Cai, W. & Yuan, W. Accurate representation of leaf longevity is important for simulating ecosystem carbon cycle. *Basic Appl. Ecol.* **17**, 396–407 (2016).
5. X. Chen et al. Vapor pressure deficit and sunlight explain seasonality of leaf phenology and photosynthesis across amazonian evergreen broadleaved forest. *Glob. Biogeochem. Cycles* **35**, e2020GB006893 (2021).
6. Tagesson, T. et al. Recent divergence in the contributions of tropical and boreal forests to the terrestrial carbon sink. *Nat. Ecol. Evol.* **4**, 202–209 (2020).
7. Chen, X. et al. Novel representation of leaf phenology improves simulation of Amazonian evergreen forest photosynthesis in a land surface model. *J. Adv. Model. Earth Syst.* **12**, e2018MS001565 (2020).
8. Guo, Y. et al. Enhanced leaf turnover and nitrogen recycling sustain CO2 fertilization effect on tree-ring growth. *Nat. Ecol. Evol.* **6**, 1271–1278 (2022).
9. Xu, X. et al. Variations of leaf longevity in tropical moist forests predicted by a trait-driven carbon optimality model. *Ecol. Lett.* **20**, 1097–1106 (2017).
10. Reich, P. B., Uhl, C., Walters, M. B., Prugh, L. & Ellsworth, D. S. Leaf demography and phenology in Amazonian rain forest: a census of 40 000 leaves of 23 tree species. *Ecol. Monographs* **74**, 3–23 (2004).
11. Gatti, R. C. azzola et al. The number of tree species on Earth. *Proc. Natl. Acad. Sci. USA* **119**, e2115329119 (2022).
12. Reich, P. B., Uhl, C., Walters, M. B. & Ellsworth, D. S. Leaf lifespan as a determinant of leaf structure and function among 23 Amazonian tree species. *Oecologia* **86**, 16–24 (1991).
13. Reich, P. B., Walters, M. B. & Ellsworth, D. S. From tropics to tundra: global convergence in plant functioning. *Proc. Natl. Acad. Sci. USA* **94**, 13730–13734 (1997).
14. Russo, S. E. & Kitajima, K. The ecophysiology of leaf lifespan in tropical forests: adaptive and plastic responses to environmental heterogeneity. in *Tropical Tree Physiology: Adaptations and Responses in a Changing Environment*, 357–383 (2016).
15. Menezes, J. et al. Changes in leaf functional traits with leaf age: when do leaves decrease their photosynthetic capacity in Amazonian trees? *Tree Physiol.* **42**, 922–938 (2022).
16. Kikuzawa, K. & Lechowicz, M. J. *Ecology of Leaf Longevity*. (Springer Science & Business Media, 2011).

17. Smith, L. et al. Leaf longevity in temperate evergreen species is related to phylogeny and leaf size. *Oecologia* **191**, 483–491 (2019).

18. Oleksyn, J. et al. A fingerprint of climate change across pine forests of Sweden. *Ecol. Lett.* **23**, 1739–1746 (2020).

19. Wang, H. et al. Leaf economics fundamentals explained by optimality principles. *Sci. Adv.* **9**, eadd5667 (2023).

20. Slot, M. et al. Thermal acclimation of leaf respiration of tropical trees and lianas: response to experimental canopy warming, and consequences for tropical forest carbon balance. *Global Change Biol.* **20**, 2915–2926 (2014).

21. Sastry, A., Guha, A. & Barua, D. Leaf thermotolerance in dry tropical forest tree species: relationships with leaf traits and effects of drought. *AoB Plants* **10**, plx070 (2018).

22. Reich, P. B. et al. Boreal and temperate trees show strong acclimation of respiration to warming. *Nature* **531**, 633–636 (2016).

23. Doughty, C. E. et al. Drought impact on forest carbon dynamics and fluxes in Amazonia. *Nature* **519**, 78–82 (2015).

24. Huang, M. et al. Air temperature optima of vegetation productivity across global biomes. *Nat. Ecol. Evol.* **3**, 772–779 (2019).

25. Kullberg, A. T. & Feeley, K. J. Limited acclimation of leaf traits and leaf temperatures in a subtropical urban heat island. *Tree Physiol.* **42**, 2266–2281 (2022).

26. Nomura, M., Hatada, A. & Itioka, T. Correlation between the leaf turnover rate and anti-herbivore defence strategy (balance between ant and non-ant defences) amongst ten species of Macaranga (Euphorbiaceae). *Plant Ecol.* **212**, 143–155 (2011).

27. Paoletti, E., Pagano, M., Zhang, L., Badea, O. & Hoshika, Y. Allocation of nutrients and leaf turnover rate in poplar under ambient and enriched ozone exposure and soil nutrient manipulation. *Biology* **13**, 232 (2024).

28. Isbell, F. et al. Biodiversity increases the resistance of ecosystem productivity to climate extremes. *Nature* **526**, 574–577 (2015).

29. Sugihara, G. et al. Detecting causality in complex ecosystems. *Science* **338**, 496–500 (2012).

30. Zhang-Zheng, H. et al. Why models underestimate West African tropical forest primary productivity. *Nat. Commun.* **15**, 9574 (2024).

31. Robin, M. et al. Interactions between leaf phenological type and functional traits drive variation in isoprene emissions in central Amazon forest trees. *Front. Plant Sci.* **15**, 1522606 (2024).

32. Veneklaas, E. J. Phosphorus resorption and tissue longevity of roots and leaves-importance for phosphorus use efficiency and ecosystem phosphorus cycles. *Plant Soil* **476**, 627–637 (2022).

33. Aguirre-Gutiérrez, J. et al. N. N. s. Bengone, Functional susceptibility of tropical forests to climate change. *Nat. Ecol. Evol.* **6**, 878–889 (2022).

34. Kikuzawa, K., Onoda, Y., Wright, I. J. & Reich, P. B. Mechanisms underlying global temperature-related patterns in leaf longevity. *Glob. Ecol. Biogeogr.* **22**, 982–993 (2013).

35. Tian, J. et al. A leaf age-dependent light use efficiency model for remote sensing the gross primary productivity seasonality over pantropical evergreen broadleaved forests. *Glob. Change Biol.* **30**, e17454 (2024).

36. Forkel, M. et al. Constraining modelled global vegetation dynamics and carbon turnover using multiple satellite observations. *Sci. Rep.* **9**, 18757 (2019).

37. Wright, S. J. et al. Functional traits and the growth–mortality trade-off in tropical trees. *Ecology* **91**, 3664–3674 (2010).

38. Cui, E., Weng, E., Yan, E. & Xia, J. Robust leaf trait relationships across species under global environmental changes. *Nat. Commun.* **11**, 2999 (2020).

39. Kikuzawa, K. The basis for variation in leaf longevity of plants. *Vegetatio* **121**, 89–100 (1995).

40. Yang, X. et al. A gridded dataset of a leaf-age-dependent leaf area index seasonality product over tropical and subtropical evergreen broadleaved forests. *Earth Syst. Sci. Data* **15**, 2601–2622 (2023).

41. Gomarasca, U. et al. Leaf-level coordination principles propagate to the ecosystem scale. *Nat. Commun.* **14**, 3948 (2023).

42. Zhang, L., Luo, T., Zhu, H., Daly, C. & Deng, K. Leaf life span as a simple predictor of evergreen forest zonation in China. *J. Biogeogr.* **37**, 27–36 (2010).

43. Hikosaka, K. A model of dynamics of leaves and nitrogen in a plant canopy: an integration of canopy photosynthesis, leaf life span, and nitrogen use efficiency. *Am. Naturalist* **162**, 149–164 (2003).

44. Hordijk, I. et al. Evenness mediates the global relationship between forest productivity and richness. *J. Ecol.* **111**, 1308–1326 (2023).

45. McGill, B. J. et al. Species abundance distributions: moving beyond single prediction theories to integration within an ecological framework. *Ecol. Lett.* **10**, 995–1015 (2007).

46. Wang, X.-Y. et al. Evenness alters the positive effect of species richness on community drought resistance via changing complementarity. *Ecol. Indicators* **133**, 108464 (2021).

47. Collalti, A. et al. Forest production efficiency increases with growth temperature. *Nat. Commun.* **11**, 5322 (2020).

48. Gunderson, C. A., O'Hara, K. H., Campion, C. M., Walker, A. V. & Edwards, N. T. Thermal plasticity of photosynthesis: the role of acclimation in forest responses to a warming climate. *Glob. Change Biol.* **16**, 2272–2286 (2010).

49. Choat, B. et al. Global convergence in the vulnerability of forests to drought. *Nature* **491**, 752–755 (2012).

50. DeSoto, L. et al. Low growth resilience to drought is related to future mortality risk in trees. *Nat. Commun.* **11**, 545 (2020).

51. Pfisterer, A. B. & Schmid, B. Diversity-dependent production can decrease the stability of ecosystem functioning. *Nature* **416**, 84–86 (2002).

52. Mouillot, D. et al. Rare species support vulnerable functions in high-diversity ecosystems. *PLoS Biol.* **11**, e1001569 (2013).

53. Neeson, T. M. et al. Conserving rare species can have high opportunity costs for common species. *Glob. Change Biol.* **24**, 3862–3872 (2018).

54. Friedl, M. D. Sulla-Menashe MODIS/Terra+ Aqua Land Cover Type Yearly L3 Global 0.05 Deg CMG V061 [Data set]. NASA EOSDIS Land Processes Distributed Active Archive Center, (Accessed 2023-10-11 from https://doi.org/10.5067/MODIS/MCD12C1.061, 2022).

55. Potapov, P. et al. The global 2000-2020 land cover and land use change dataset derived from the Landsat archive: first results. *Front. Remote Sens.* **3**, 856903 (2022).

56. Su, Y. et al. Asymmetric influence of forest cover gain and loss on land surface temperature. *Nat. Clim. Change* **13**, 823–831 (2023).

57. Chuvieco, E., Pettinari, M. L., Lizundia Loiola, J., Storm, T., Padilla Parellada, M. ESA Fire climate change initiative (Fire_cci): MODIS Fire_cci burned area grid product, version 5.1. (2019).

58. Tao, S. et al. Increasing and widespread vulnerability of intact tropical rainforests to repeated droughts. *Proc. Natl. Acad. Sci. USA* **119**, e2116626119 (2022).

59. Palmer, W. C. *Meteorological drought.*, vol. 30 (US Department of Commerce, Weather Bureau, 1965).

60. Vicente-Serrano, S. M., Beguería, S. & López-Moreno, J. I. A multiscalar drought index sensitive to global warming: the standardized precipitation evapotranspiration index. *J. Clim.* **23**, 1696–1718 (2010).

61. Aragão, L. E. O. C. et al. Spatial patterns and fire response of recent Amazonian droughts. *Geophys. Res. Lett.* **34**, https://doi.org/10.1029/2006GL028946 (2007).

62. Liu, L. et al. Tropical tall forests are more sensitive and vulnerable to drought than short forests. *Glob. Change Biol.* **28**, 1583–1595 (2022).

63. Farquhar, G. D., von Caemmerer, S. V. & Berry, J. A. A biochemical model of photosynthetic CO_2 assimilation in leaves of C3 species. *Planta* **149**, 78–90 (1980).

64. Wu, J. et al. Partitioning controls on Amazon forest photosynthesis between environmental and biotic factors at hourly to interannual timescales. *Glob. Change Biol.* **23**, 1240–1257 (2017).

65. Wu, J. et al. The phenology of leaf quality and its within-canopy variation is essential for accurate modeling of photosynthesis in tropical evergreen forests. *Glob. Change Biol.* **23**, 4814–4827 (2017).

66. Li, X. & Xiao, J. Mapping photosynthesis solely from solar-induced chlorophyll fluorescence: a global, fine-resolution dataset of gross primary production derived from OCO-2. *Remote Sensing.* https://doi.org/10.3390/rs11212563 (2019).

67. Milliman, T. et al. PhenoCam Dataset v2. 0: digital camera imagery from the phenoCam network, 2000–2018. *ORNL Distributed Active Archive Center* (2019).

68. Botía, S. et al. The CO_2 record at the Amazon Tall Tower Observatory: A new opportunity to study processes on seasonal and inter-annual scales. *Glob. Change Biol.* **28**, 588–611 (2022).

69. Eschenbach, C. & Kappen, L. Leaf area index determination in an alder forest: a comparison of three methods. *J. Exp. Botany* **47**, 1457–1462 (1996).

70. Wang, C. et al. Scaling relationships between the total number of leaves and the total leaf area per culm of two dwarf bamboo species. *Ecol. Evol.* **14**, e70002 (2024).

71. Li, Q. et al. Remote sensing of seasonal climatic constraints on leaf phenology across pantropical evergreen forest biome. *Earth's Future* **9**, e2021EF002160 (2021).

72. Negrón Juárez, R. I. & Liu, W. T. FFT analysis on NDVI annual cycle and climatic regionality in Northeast Brazil. *Int. J. Climatol. A J. R. Meteorol. Soc.* **21**, 1803–1820 (2001).

73. Yu, B. & Silva, C. T. VisFlow-Web-based visualization framework for tabular data with a subset flow model. *IEEE Trans. Vis. Comput. Graph.* **23**, 251–260 (2016).

74. Otto, E. et al. Overview of Sankey flow diagrams: Focusing on symptom trajectories in older adults with advanced cancer. *J. Geriatric Oncol.* **13**, 742–746 (2022).

75. Hair, J. F., Risher, J. J., Sarstedt, M. & Ringle, C. M. When to use and how to report the results of PLS-SEM. *Eur. Business Rev.* **31**, 2–24 (2019).

76. Mateos-Aparicio, G. Partial least squares (PLS) methods: Origins, evolution, and application to social sciences. *Commun. Stat. Theor. Meth.* **40**, 2305–2317 (2011).

77. Evermann, J. & Tate, M. Assessing the predictive performance of structural equation model estimators. *Journal of Business Research* **69**, 4565–4582 (2016).

78. Sarstedt, M., Ringle, C. M. & Hair, J. F. in *Handbook of Market Research.* 587–632 (Springer, 2021).

79. Zhong, Z. et al. Disentangling the effects of vapor pressure deficit on northern terrestrial vegetation productivity. *Sci. Adv.* **9**, eadf3166 (2023).

80. Purwanto, A. & Sudargini, Y. Partial least squares structural equation modeling (PLS-SEM) analysis for social and management research: a literature review. *J. Ind. Eng. Manag. Res.* **2**, 114–123 (2021).

81. Ravand, H. & Baghaei, P. Partial least squares structural equation modeling with R. *Practical Assessment. Res. Eval.* **21**, n11 (2016).

82. Abatzoglou, J. T., Dobrowski, S. Z., Parks, S. A. & Hegewisch, K. C. TerraClimate, a high-resolution global dataset of monthly climate and climatic water balance from 1958–2015. *Sci. Data* **5**, 1–12 (2018).

83. Ryu, Y., Jiang, C., Kobayashi, H. & Detto, M. MODIS-derived global land products of shortwave radiation and diffuse and total photosynthetically active radiation at 5km resolution from 2000. *Remote Sens. Environ.* **204**, 812–825 (2018).

84. Muñoz Sabater, J. ERA5-Land monthly averaged data from 1981 to present. *Copernicus Climate Change Service (C3S) Climate Data Store (CDS)* **10** (2019).

85. Tropical Rainfall Measuring Mission (TRMM), TRMM (TMPA/3B43) Rainfall Estimate L3 1 month 0.25 degree x 0.25 degree V7, Greenbelt, MD, Goddard Earth Sciences Data and Information Services Center (GES DISC), Accessed: [*Data Access Date*], https://doi.org/10.5067/TRMM/TMPA/MONTH/7 (2011).

86. Myles, A. J., Feudale, R. N., Liu, Y., Woody, N. A. & Brown, S. D. An introduction to decision tree modeling. *J. Chemom. A J. Chemom. Soc.* **18**, 275–285 (2004).

87. Hobley, E., Wilson, B., Wilkie, A., Gray, J. & Koen, T. Drivers of soil organic carbon storage and vertical distribution in Eastern Australia. *Plant Soil* **390**, 111–127 (2015).

88. Yang, H. et al. Climatic and biotic factors influencing regional declines and recovery of tropical forest biomass from the 2015/16 El Niño. *Proc. Natl. Acad. Sci. USA* **119**, e2101388119 (2022).

89. Breiman, L. Random forests. *Mach. Learn.* **45**, 5–32 (2001).

90. Segal, M. R. Machine learning benchmarks and random forest regression. (2004).

91. Kashani, A. T. & Mohaymany, A. S. Analysis of the traffic injury severity on two-lane, two-way rural roads based on classification tree models. *Safety Sci.* **49**, 1314–1320 (2011).

92. Mitchell, T. M., Mitchell, T. M. *Machine Learning.*, vol. 1 (McGraw-hill New York, 1997).

93. Ahmadlou, M., Delavar, M. R. & Tayyebi, A. Comparing ANN and CART to model multiple land use changes: A case study of Sari and Ghaem-Shahr cities in Iran. *J. Geomatics Sci. Technol.* **6**, 292–303 (2016).

94. Janitza, S., Strobl, C. & Boulesteix, A.-L. An AUC-based permutation variable importance measure for random forests. *BMC Bioinform.* **14**, 1–11 (2013).

95. Friedman, J. H. Greedy function approximation: a gradient boosting machine. *Ann. Stat.* **29**, 1189–1232 (2001).

96. Lopes, A. P. et al. Leaf flush drives dry season green-up of the Central Amazon. *Remote Sens. Environ.* **182**, 90–98 (2016).

97. Bradley, A. V. et al. Relationships between phenology, radiation and precipitation in the Amazon region. *Glob. Change Biol.* **17**, 2245–2260 (2011).

98. Van der Tol, C., Verhoef, W. & Rosema, A. A model for chlorophyll fluorescence and photosynthesis at leaf scale. *Agric. For. Meteorol.* **149**, 96–105 (2009).

99. Mendes, K. R. & Marenco, R. A. Leaf traits and gas exchange in saplings of native tree species in the Central Amazon. *Sci. Agric.* **67**, 624–632 (2010).

100. Gloor, M. et al. Recent Amazon climate as background for possible ongoing and future changes of Amazon humid forests. *Glob. Biogeochem. Cycles* **29**, 1384–1399 (2015).

101. Betts, R. A., Malhi, Y. & Roberts, J. T. The future of the Amazon: new perspectives from climate, ecosystem and social sciences. *Phil. Trans. R. Soc. B Biol. Sci.* **363**, 1729–1735 (2008).

102. Esquivel-Muelbert, A. et al. Tree mode of death and mortality risk factors across Amazon forests. *Nat. Commun.* **11**, 5515 (2020).

103. McDowell, N. et al. Drivers and mechanisms of tree mortality in moist tropical forests. *N. Phytol.* **219**, 851–869 (2018).

104. Aguirre-Gutiérrez, J. et al. Canopy functional trait variation across Earth's tropical forests. *Nature* **641**, 129–136 (2025).

105. Malhi, Y. et al. The Global Ecosystems Monitoring network: Monitoring ecosystem productivity and carbon cycling across the tropics. *Biol. Conserv.* **253**, 108889 (2021).

106. Blundo, C. et al. Taking the pulse of Earth's tropical forests using networks of highly distributed plots. *Biol. Conserv.* **260**, 108849 (2021).

107. Kattge, J. et al. TRY plant trait database - enhanced coverage and open access. *Glob. Change Biol.* **26**, 119–188 (2020).

108. Running, S., Mu, Q. & Zhao, M. MOD17A2H MODIS/terra gross primary productivity 8-day L4 global 500m SIN grid V006 (2015).

109. Chen, J. M. et al. Global datasets of leaf photosynthetic capacity for ecological and earth system research. *Earth Syst. Sci. Data* **14**, 4077–4093 (2022).

110. Jung, M. et al. Compensatory water effects link yearly global land CO_2 sink changes to temperature. *Nature* **541**, 516–520 (2017).

111. Zheng, Y. et al. Improved estimate of global gross primary production for reproducing its long-term variation, 1982–2017. *Earth Syst. Sci. Data* **12**, 2725–2746 (2020).

112. Bi, W. et al. A global 0.05° dataset for gross primary production of sunlit and shaded vegetation canopies from 1992 to 2020. *Sci. Data* **9**, 213 (2022).

113. Zhang, Y. et al. A global moderate resolution dataset of gross primary production of vegetation for 2000-2016. *Sci. Data* **4**, 170165 (2017).

114. Badgley, G., Anderegg, L. D. L., Berry, J. A. & Field, C. B. Terrestrial gross primary production: Using NIRV to scale from site to globe. *Glob. Change Biol.* **25**, 3731–3740 (2019).

115. De Kauwe, M. G. et al. A test of the 'one-point method' for estimating maximum carboxylation capacity from field-measured, light-saturated photosynthesis. *N. Phytol.* **210**, 1130–1144 (2016).

116. Harris, I., Jones, P. D., Osborn, T. J. & Lister, D. H. Updated high-resolution grids of monthly climatic observations-the CRU TS3. 10 Dataset. *Int. J. Climatol.* **34**, 623–642 (2014).

117. Liang, J. et al. Positive biodiversity-productivity relationship predominant in global forests. *Science* **354**, aaf8957 (2016).

118. Moesinger, L. et al. The global long-term microwave vegetation optical depth climate archive (VODCA). *Earth Syst. Sci. Data* **12**, 177–196 (2020).

119. Li, X. et al. Temporal trade-off between gymnosperm resistance and resilience increases forest sensitivity to extreme drought. *Nat. Ecol. Evol.* **4**, 1075–1083 (2020).

120. Yao, Y. et al. Declining tradeoff between resistance and resilience of ecosystems to drought. *Earth's Future* **12**, e2024EF004665 (2024).

Acknowledgements

Author contributions

X.C.: conceptualization, methodology, funding acquisition, supervision, and writing. M.X. and X.Y.: methodology, visualization, data processing, formal analysis, and writing. C.W.: methodology, review and editing. P.C., L.Z., P.B.R., J.X., X.L., X.X., J.K.G., J.M.C., J.L., J.S., X.Z.L., J.T., H.L., P.Z., K.Y., X.F., L.H., and W.Y.: review and editing. All authors contributed to the discussion and commented on the manuscript.

Competing interests

The authors declare no competing interests.

Additional information

Supplementary information The online version contains supplementary material available at https://doi.org/10.1038/s41467-026-68989-x.

Correspondence and requests for materials should be addressed to Xiuzhi Chen or Chaoyang Wu.

Peer review information *Nature Communications* thanks Hamdi Zurqani and the other anonymous reviewer(s) for their contribution to the peer review of this work. A peer review file is available.

Reprints and permissions information is available at http://www.nature.com/reprints

Publisher's note Springer Nature remains neutral with regard to jurisdictional claims in published maps and institutional affiliations.

[1]Guangdong Province Data Center of Terrestrial and Marine Ecosystems Carbon Cycle, School of Atmospheric Sciences, School of Ecology, Sun Yat-sen University, Zhuhai, China. [2]Department of Land Surveying and Geo-Informatics, The Hong Kong Polytechnic University, Hong Kong, China. [3]Laboratoire des Sciences du Climat et de l'Environnement, IPSL, CEA-CNRS-UVSQ, Université Paris-Saclay, Gif sur Yvette, France. [4]Department of Atmospheric and Environmental Sciences, University at Albany, State University of New York, Albany, NY, USA. [5]Institute for Global Change Biology and School for Environment and Sustainability, University of Michigan, Ann Arbor, USA. [6]Department of Forest Resources, University of Minnesota, St. Paul, USA. [7]Earth Systems Research Center, Institute for the Study of Earth, Oceans, and Space, University of New Hampshire, Durham, NH, USA. [8]School of Geography and Planning, Guangdong Key Laboratory for Urbanization and Geo-simulation, Sun Yat-sen University, Guangzhou, China. [9]Department of Microbiology and Plant Biology, Center for Earth Observation and Modeling, University of Oklahoma, Norman, OK, USA. [10]Department of Environmental Science, University of Arizona, Tucson, AZ, USA. [11]Department of Geography and Planning, University of Toronto, Ontario, Canada. [12]Ottawa Research and Development Centre, Agriculture and Agri-Food Canada, Ontario, Canada. [13]Department of Geography, National University of Singapore, Singapore, Singapore. [14]South China Botanical Garden, Chinese Academy of Sciences, Guangzhou, China. [15]Department of geography, The University of Hong Kong, Hong Kong, China. [16]State Key Laboratory of Remote Sensing and Digital Earth, Advanced Interdisciplinary Institute of Satellite Applications, Faculty of Geographical Science, Beijing Normal University, Beijing, China. [17]School of Civil Engineering and Geomatics, Shandong University of Technology, Zibo, China. [18]Institute of Carbon Neutrality, College of Urban and Environmental Sciences, Peking University, Beijing, China. [19]Institute of Geographical Sciences and Natural Resources Research, Chinese Academy of Sciences, Beijing, China. [20]These authors contributed equally: Meimei Xue, Xueqin Yang. ✉e-mail: chenxzh73@mail.sysu.edu.cn; wucy@igsnrr.ac.cn